Monitoring Microwave Thermal Ablation using Electrical Impedance Tomography: an experimental feasibility study

Anna Bottiglieri[1], Eoghan Dunne[1], Barry McDermott[1], Marta Cavagnaro[3], Emily Porter[2], Laura Farina[2,4]

[1] Department of Electrical and Electronic Engineering, National University of Ireland Galway, Galway, Ireland, a.bottiglieri1@nuigalway.ie

[2] Translational Medical Device Lab, National University of Ireland Galway, Ireland

[3] Department of Information Engineering, Electronics and Telecommunications, Sapienza University of Rome, Italy

[4] CÚRAM, SFI Research Centre for Medical Devices, Galway, Ireland

***Abstract*—Low-cost and reliable methods for monitoring the size of the ablation zone during microwave thermal ablation (MTA) are crucial in the oncological clinical practice. The aim of this work is to test the performance of electrical impedance tomography (EIT) for the real-time monitoring of the ablation area where relevant temperature increases occur. In this work, two experimental studies were performed with a 16-electrode EIT system using a liver-mimicking agar phantom. First, an EIT system was tested to monitor the cooling of the phantom from an initial temperature of about 72˚C. Secondly, the heating and the consequent cooling of the phantom were monitored. The heating was performed using the MTA applicator operating at 30W for 10 minutes at 2.45GHz. The results reporting the voltage and temperature data acquired, as well as the reconstructed time series images, confirm the feasibility of EIT to monitor the changes of the electrical conductivity with temperature.**

***Index Terms*—microwave thermal ablation, electrical impedence tomography, image reconstruction, electrical conductivity, temperature.**

I. INTRODUCTION

Microwave thermal ablation (MTA) is a well-established technique used to treat solid tumours such as hepatocellular carcinoma, renal tumours, lung tumours and bony lesions [1]. During the MTA procedure, an antenna operating generally at 915 MHz or 2.45 GHz is inserted in the target region. The electromagnetic field radiated by the antenna is absorbed by the biological tissue. The consequent increase of the temperature within 50 – 60˚C triggers biological mechanisms (e.g. protein denaturation, cell membrane destruction) inducing the rapid cellular death of the tissue under treatment [2], [3].

In order to obtain satisfying results during the MTA procedure, the ablation area (i.e. the area where the temperature exceeds 50 - 60˚C) should completely cover the tumour region (plus a safety margin of at least 5 mm [2]). Moreover, the healthy tissue around the tumour should be preserved from excessive temperature increase [4], [5]. In this context, real-time monitoring of the ablation procedure is needed to control the size of the ablation zone and the related temperature increase [6]. The continuous monitoring of the ablation procedure aims at achieving complete ablation in the tissue target, in particular in cases where blood vessels could cause a heat sink effect and consequently cause an inhomogeneous ablation zone. A further goal is to prevent undesired overheating and damage to the surrounding healthy tissue, in the cases where the target is in proximity to critical structures (e.g. diaphragm, vital blood vessels, functional tissues) [6] − [8].

The main techniques currently used to monitor ablation treatments generally involve ultrasound (US), computed tomography (CT) or magnetic resonance imaging (MRI) [8], [9], [10]. The high intensity focused ultrasound technique requires a skilled operator to treat localised tumour during the MTA treatment due to the echogenic scatter induced by the vapour generated in the tissue target caused by the increase of temperature. MRI using proton frequency resonance can provide highly sensitive temperature distributions with accurate spatial resolution. However, the MRI requires the antenna to be MRI compatible and considerable costs. In the case of CT, the principal drawback is related to the ionizing radiation dose provided to the patient and potentially to the operator. Thus, CT is commonly used to assess the antenna positioning and the ablation zone pre- and post- treatment, respectively; but not for real-time monitoring. Following the above, MTA procedures lack of a reliable, non-invasive, and cost-effective method for real time monitoring of the evolving thermal ablation area [11]. Recent studies investigated applicability of microwave imaging to derive, from the changes in the dielectric properties of tissues induced by the temperature increase [12], the map of the temperature in the treated area [13], [14].

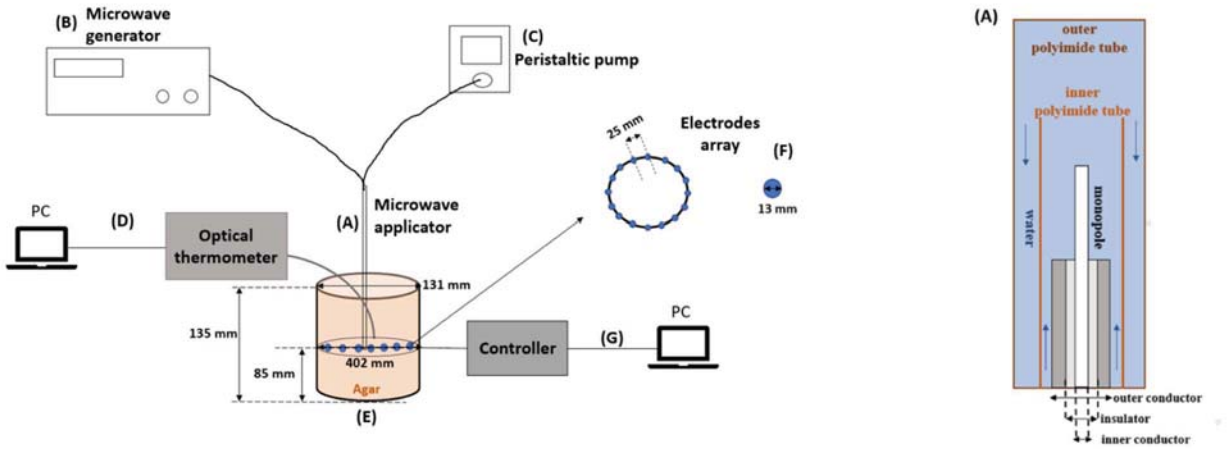

Fig. 1: Experimental setup including: the monopole-based microwave antenna operating at 2.45 GHz and equipped by an integrated cooling system (A), the microwave generator powering the antenna at 30 W for 10 min (B), a peristaltic pump connected to the integrated cooling system of the applicator (C), the optical thermometer (D) placed inside the agar phantom (E) and the ring of electrodes (F) connected to EIT system.

Electrical impedance tomography (EIT) is a low cost and non-ionizing radiation imaging method that could represent a valuable alternative to the traditional imaging techniques for the monitoring of the thermal ablation treatments [15], [16]. Over the past years, EIT has been adopted in the monitoring of the bladder volume [17], the cardiac stroke volume [18], the brain function [19], the pulmonary regional ventilation [20] and in cancer imaging [21], [22]. The technology is based on the injection of small alternating currents through electrodes surrounding the region of interest and on the following measurement of the resultant surface voltages. The monitoring of the target region is performed through analysis of these collected voltages and, consequently, through the interpretation of the reconstructed images of the area under test.

In this paper, EIT is used: 1) to monitor the changes of the electrical conductivity during the cooling of an agar phantom measuring approximately 128 mm in diameter and 135 mm in height, 2) to identify the changes in the electrical conductivity induced by microwave heating in the agar phantom.

II. Methodology

The experimental setup includes a non-perfectly cylindrical (i.e. the circumference changes with the height of the tank) tank measuring 412 mm circumference (at the height of the electrode ring), 131 mm inner diameter and 135 mm height. The tank is surrounded by 16 equally spaced electrodes (two consecutive electrodes are about 25 mm apart) placed at 85 mm from the lower boundary of the tank (Fig. 1).

In the first experimental scenario, an agar phantom mimicking liver dielectric property at 2.45 GHz was made by: 1700 ml deionised water, 17 g NaCl, 17 g sucrose and 170 g agar powder (i.e. 10% of the water weight) (Fisher BioReagents™, Thermo Fisher Scientific, Waltham, MA, U.S) [23]. The mixture was heated up to about 72˚C, and, while at this temperature (72˚C), it was poured in the above-mentioned tank up to a height of 135 mm. Then, the raw EIT data and temperature data were recorded for around 60 min during the cooling of the phantom.

In the second experimental scenario, MTA was performed on the agar phantom (10%, i.e. made with the same recipe above described). A fully cooled coaxial-based monopole antenna (outer diameter = 1.2 mm; insulator = 0.9 mm; inner diameter = 0.3 mm) optimized to work at 2.45 GHz was placed in the centre of the tank. A cooling system prevents the overheating along the applicator cable and the detuning between the antenna and the material under test during the MTA. The applicator is connected to a peristaltic pump (DP2000, Thermo-Fisher Scientific Inc., Waltham, Massachusetts, US) circulating water at 18˚C at 50 ml/min; and to a microwave generator (Sairem, SAS, France) operating at 2.45 GHz frequency, through a low-loss coaxial cable (50 Ohm characteristic impedance). The antenna was powered at 30 W for 10 min. The raw EIT data and temperature data were recorded simultaneously during the ablation treatment (10 min) and for 20 minutes after the heating source was switched off.

In each experimental study, the temperature data were acquired over time at 0.1 s time steps using a fibre optic sensor (Neoptix Inc., Québec, CA) that was inserted in the sample under test and maintained approximately in the middle of the circular electrodes array. The optical thermometer was connected to a laptop. Post-processing after the experimental session included a moving average operation (0.4% percentage error between the actual data and the averaged data) performed to minimise the environmental noise overlapping the measured data.

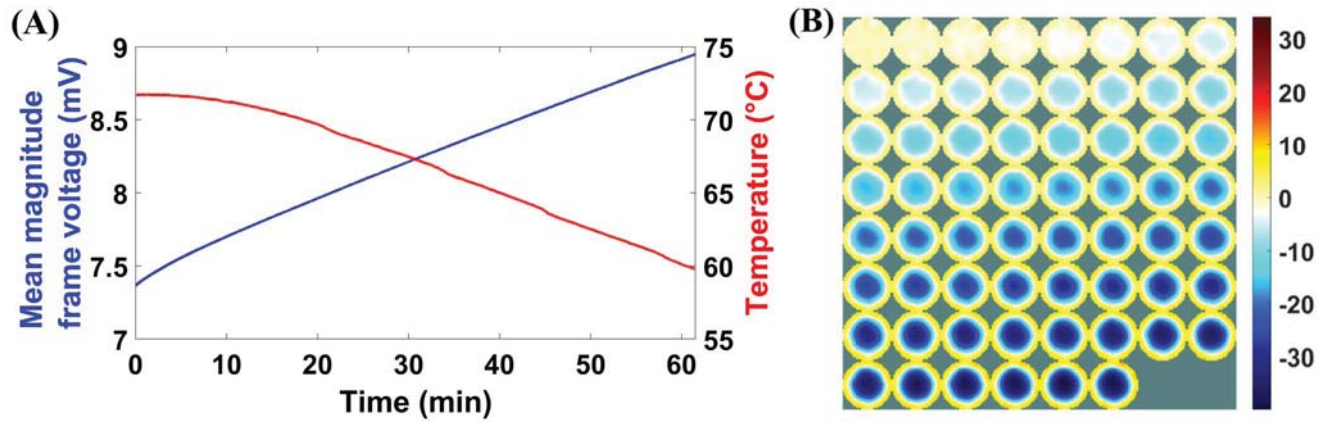

Fig.2: Temperature (blue line) and voltage (red line) data related to the cooling of the agar phantom acquired over 62 min (Fig. A); time series images at 60 seconds step intervals reconstructed with GREIT representing the physical changes in the medium during the cooling of the phantom (Fig. B).

The system dedicated to acquiring the temperature data and the EIT system were manually synchronised.

EIT data were recorded with a calibrated Sentec (formally Swisstom) Pioneer EIT set (Sentec.com, Switzerland) using small alternating currents (6 mA_{p-p}) at an injection frequency of 45 kHz with a skip (i.e. the gap between the injection electrodes) of four electrodes. This EIT system is designed for 32 electrodes. In this study, due to the small tank diameter, post-processing was performed on the signals recorded by 16 electrodes only. The voltage frame data (i.e. EIT data acquired during one cycle of current applications and voltage measurements) were collected with a rate of 14.96 frames/s.

The raw EIT data recorded during each experiment were loaded using the open-source EIT and Diffuse Optical tomography Reconstruction Software (EIDORS) [24] 3.9.1 and the Sentec .eit file reader. EIDORS was used to remove injection electrode measurements leading to 208 (n×n-3×n where n = 16 electrodes) measurements per frame. For image reconstruction, the commonly employed time-difference algorithm GREIT was used with a noise figure of 0.5 [25]. In the case of the cooling of the agar phantom, the reference measurement was the mean of the first 10 frames acquired in the recording. During the experiment involving the MTA of the phantom, the reference frame was the mean of the first 10 frames recorded at the start of the ablation. The image reconstruction was carried out using a finite element model (FEM) representing the tank with circular surface electrodes and a homogeneous background conductivity of 1 S/m.

III. Results and Discussion

In this study, an agar phantom was used to test the performance of EIT in detecting the electrical conductivity changes related to the temperature. The main goal of this study was to use EIT in the detection of the changes occurring during MTA.

First a preliminary experiment was conducted to test the capability of the EIT system in monitoring the changes in temperature occurring during the cooling of the agar phantom. During this experiment, the initial high temperature of the material under test was achieved using a hot plate. The results of this first experiment are reported in Fig. 2. Fig. 2(A) shows the mean magnitude voltage (over the 208 measurements per frame at each time step of about 0.067 s) and the temperature data acquired during the cooling of the agar phantom (62 min). The initial temperature of the agar phantom measured by the fibre optic sensor was 71.7˚C. After 62 min, the internal temperature of the phantom detected by the thermal sensor was 59.8˚C. Thus, a 19.9% difference between the initial temperature and the final temperature was observed. As the electrical conductivity is related to the movements of the ions in the material under test, this parameter decreases over the observation time with the cooling of the material. In the EIT system, the decrease of the electrical conductivity induces an increase in the voltage measured by the electrodes around the tank, as the system is current-controlled (fixed injection current). The percentage difference between the initial and the final mean voltage value over 62 min is 21.5%. Fig. 2(B) shows the reconstructed images displaying the variation in conductivity every 60 s. Progressive changes in the phantom under test related to the decrease of the temperature are observed over 62 min. The colourbar represents the pixel intensity: lower intensity corresponds to smaller changes in conductivity and higher intensity corresponds to larger changes. The distribution of the cooling in the material under test could be related to thermodynamic effects linked with the presence of a thick insulating material, such as plastic, at the boundary.

After the preliminary experiment related to the cooling of the agar phantom, the EIT system was used to acquire changes in voltage values induced by MTA, during and after the heating. Fig. 3 shows the related results. In particular, Fig. 3(A) shows temperature and voltage data acquired over about 35 min. From Fig. 3(A) an approximately constant voltage and

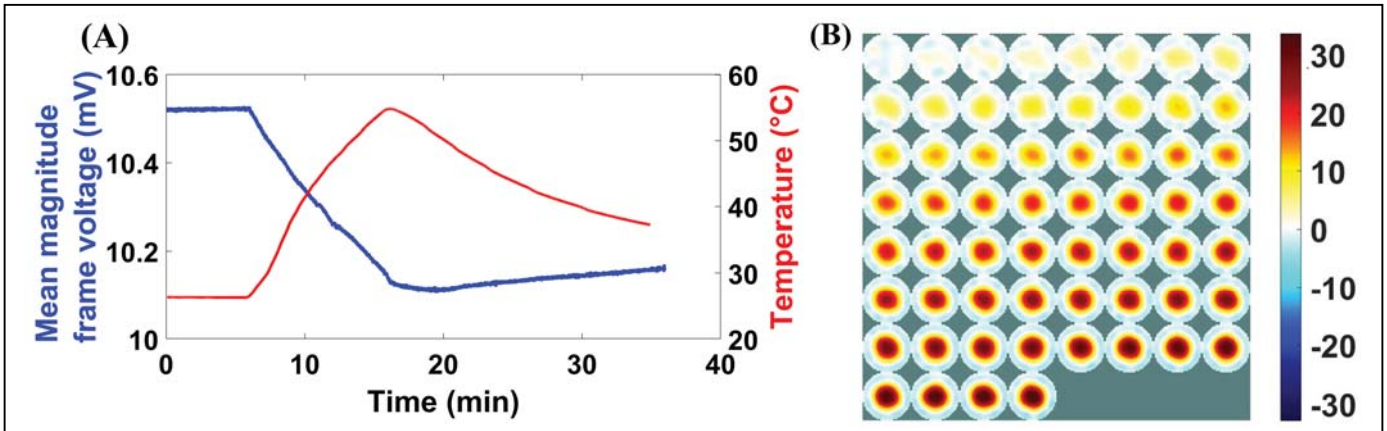

Fig. 3: A: Temperature (blue line) and voltage (red line) data acquired over about 2100 s (35 min). MTA was performed from around 360 s to 971 s (i.e. approximately 10 min). Time series reconstructed images at about 10 s time steps related only to the time when the MTA was conducted (Fig. B).

temperature over the first 6 min, when only the EIT system and the cooling system of the microwave applicator were switched on, can be derived (i.e. the heating source was off). Then, the decrease in voltage and increase in temperature during 10 min of ablation (up to 16 min in Fig. 3(A)) are shown. The increase of temperature due to the delivery of the microwave energy into the material induces an increase of the movement of the ions in the phantom. Accordingly, the progressive increase of the electrical conductivity of the agar phantom induces the decrease of the voltage measured from the electrodes. When the microwave generator is switched off, the percentage differences of the temperature values and the voltage values are 51.6% and 4%, respectively. As the extent of the area heated during the MTA is smaller compared to the area involved in the cooling process (first experimental study), a smaller percentage difference in the mean magnitude voltage values (4%) is observed. During the 20 min (from 16 min to 35 min in Fig. 3(A)) after the MTA, the temperature values decrease, whereas the increase of the voltage is about 0.3%. This result suggests an irreversible change in the composition of the agar phantom. As the temperature detected is around 55˚C, a loss of the original water content inside the phantom is reasonably the cause of the quasi-permanent change of the electrical conductivity of the material.

In Fig. 3(B), the time series of the reconstructed images at 10 s time intervals are reported. The reconstructed images are presented for the time interval during the MTA. The rapid change of the electrical conductivity due to applied MW energy is seen for approximately 10 min. In particular, Fig. 3(B) shows the progressive increase of the size of the region where conductivity changes occurred, pointing out a relation between the changes in the properties (i.e. electrical conductivity) of the material under test and its temperature changes.

These results support the hypothesis of exploiting EIT to monitor the heating patterns and the ablation effects during the ablation therapy. Further investigation is needed to optimize the imaging algorithm for this specific application, and future work also will include shifting the position of the MTA applicator from the centre of the phantom. Application of the EIT system to ablation of *ex vivo* samples is also planned. Moreover, a further improvement will include a second ring of electrodes at a different height in order to capture 3D information that may enhance data collection and, possibly, improve the spatial resolution. Finally, in future studies a comprehensive investigation concerning the electrical conductivity values at EIT frequencies of the background medium is required in order to optimize the accuracy of the image reconstruction.

IV. Conclusion

Monitoring of the conductivity changes related to the temperature using EIT was investigated in this study. The results reported show the feasibility of using EIT to estimate the area undergoing a relevant conductivity change induced by a temperature change. The main application of the technique presented in this work concerns the estimation of an induced thermal ablation zone.

EIT could represent a non-invasive, feasible and economically sustainable alternative technique for the real-time monitoring (e.g. in terms of temperature distribution) and the assessment of the ablation zone in order to reduce recurrence rates.

Acknowledgment

The research leading to these results has received funding from the European Research Council under the European Union's Horizon 2020 Programme (H2020)/ERC grant agreement n.637780 and ERC PoC Grant REALTA n.754308. This publication has emanated from research conducted with the financial support of Science Foundation Ireland (SFI) and is co-funded under the European Regional Development Fund under Grant Number 13/RC/2073. This project has received funding from the European Union Horizon 2020 research and innovation programme under the Marie Skłodowska-Curie grant agreement No 713690.

V. REFERENCES

[1] N. S. Goldberg, et al., "Thermal Ablation Therapy for Focal Malignancy: a unified approach to underlying principles, techniques and diagnostic imaging guidance," *American Journal of Roentgenology,* vol. 174, no. 2, pp. 323-331, 2000.

[2] M. Ahmed, et al., "Principles and Advances in Percutaneous Ablation," *Radiology,* vol. 258, no. 2, pp. 351-369, 2011.

[3] S. Curto, et al., "Microwave ablation at 915 MHz vs 2.45 GHz: a theoretical and experimental investigation," *Med. Phys.,* vol. 42, no. 11, pp. 6152-6161, 2015.

[4] M. G. Lubner, et al., "Microwave Tumor Ablation: Mechanism of Action, Clinical Results and Devices," *J. Vasc. Interv. Radiol.,* vol. 21, no. 8, pp. 192-203, 2010.

[5] M. Ahmed, "Image Guided Tumour Ablation: Standardization of Terminology and Reporting Criteria - A 10 Year Update," *Radiology,* vol. 273, no. 1, pp. 241-260, 2014.

[6] K. Yamakado, "Image-Guided Ablation of Adrenal Lesions," *Semin. Interv. Radiol.,* vol. 31, no. 2, pp. 149-156, 2014.

[7] Y. Wang, et al., "Ultrasound-guided percutaneous micorwave ablation of adrenal metastasis: preliminary results," *International Journal of Hyperthermia,* vol. 25, no. 6, pp. 455-461, 2009.

[8] F. J. Wolf, et al., "Adrenal neoplasm: effectiveness and safety of CT-guided ablation of 23 tumors in 22 patients," *European Journal of Radiology ,* vol. 81, no. 8, pp. 1717-1723, 2012.

[9] F. A. Jolesz, et al., "Noninvasive thermal ablation of hepatocellular carcinoma by using magnetic resonance imaging-guided focused ultrasound," *Gastroenterology,* vol. 127, no. 5, pp. 242-247, 2004.

[10] L. Dalong et al., "Real-Time 2D temperature imaging using ultrasound," *IEEE Trans Biomed Eng,* vol. 57, no. 1, pp. 12-16, 2010.

[11] V. Lopresto et al., "Treatment planning in microwave thermal ablation: clinical gapsand recent research advances," *Int. J. Hyperth.,* vol. 33, no. 1, pp. 83-100, 2017.

[12] G. Ruvio et al., "Comparison of coaxial open-ended probe based dielectric measurements on ex-vivo thermally ablated liver tissue," in *13th European Conference on Antennas and Propagation (EuCAP)*, Krakow, Poland, 2019.

[13] R. Scapaticci et al., "Exploiting microwave imaging methods for real-time monitoring of thermal ablation," *Int. J. Antenn. Propag.,* pp. 1-13, 2017.

[14] R. Scapaticci et al., "Monitoring thermal ablation via microwave tomography: an ex vivo experiment assessment," *Diagnostics,* vol. 8, no. 4, pp. 1-18, 2018.

[15] H. Wi et al., "Real-time conductivity imaging of temperature and tissue property changes during radiofrequency ablation: an ex vivo model using weighted frequency difference," *Bioelectromagnetics,* vol. 36, no. 4, pp. 277-286, 2015.

[16] K. Katrioplas et al., "Monitoring of microwave ablation treatment with electrical impedance tomography," in *EMF-Med 1st World Conference on Biomedical Applications of Electromagnetic Fields* , Split, Croatia, 2018.

[17] E. Dunne et al.,"Image-based classification of bladder state using elertical impedance tomography," *Physiological Measurement,* vol. 39, no. 12, pp. 124001-124013, 2018.

[18] S. Zlochiver, D. Freimark, M. Arad, A. Adunsky and S. Abboud, "Parametric EIT for monitoring cardiac stroke volume," *Physiol. Meas.,* vol. 27, no. 5, pp. 139-146, 2006.

[19] D. S. Holder, "Electrical Impedance Tomography (EIT) of brain function," *Brain Tomography,* vol. 5, no. 2, pp. 87-93, 1992.

[20] I. Frerichs et al., "Electrical impedance tomography imaging of the cardiopulmonary system," *Curr. Opin. Crit. Care,* vol. 20, no. 3, pp. 323-332, 2014.

[21] T. L. Muftuler et al., "Resolution and contrast in magnetic resonance electrical impedance tomography (MREIT) and its application to cancer imaging," *Technology in Cancer Research and Treatment ,* vol. 3, no. 6, pp. 599-609, 2004.

[22] M. J. Moskowitz et al., "Clinical implementation of electrical impedance tomography with hyperthermia," *International Journal of Hyperthermia,* vol. 11, no. 2, pp. 141-149, 1995.

[23] L. Farina et al., "Characterisation of tissue shrinkage during microwave thermal ablation," *Int. J. Hyperth.,* vol. 30, no. 7, pp. 419-428, 2014.

[24] A. Adler et al., "Uses and abuses of EIDORS: an extensible software base for EIT," *Physiol. Meas. ,* vol. 27, no. 5, pp. S25-42, 2006.

[25] A. Adler et al., "GREIT: a unified approach to 2D linear EIT reconstruction of lung images," *Physiol. Meas. ,* vol. 30, no. 6, pp. S35-55, 2009.